

The Nature of the Vela Supernova Remnant as Revealed by O VI and C IV Absorption

Highly ionized gas, in particular C IV and O VI, is produced in the interstellar medium in regions with hot ($T \sim 10^6$ K) X-ray emitting gas and at the boundaries where hot gas and cooler ($T \sim 10^4$ K) gas interact. Supernova remnant shocks produce most of the hot gas in the ISM and, if they are in the correct range of speeds, should produce observable quantities of C IV and O VI absorption. In turn, the column densities of these ions are potentially powerful diagnostics of the shock speed and interstellar environment in which the SNR is evolving. With the advent of FUSE, the power of this diagnostic technique is now available.

Data Analysis

We have FUSE data toward 8 stars behind the Vela SNR, and have developed a data reduction and analysis method that produces reasonably reliable O VI column densities, in spite of the complexities of the FUSE spectra in this region.

Models

In order to gain insight into the observational results, the Vela SNR evolution was modelled using Piecewise Parabolic Method numerical hydrodynamics code. The code is 1-D and incorporates non-equilibrium ionization, radiative cooling, thermal conduction and magnetic pressure.

The initial runs were made using the O VI and C IV data for 3 stars in the western region of the Vela SNR, assuming a uniform ambient medium. The result, after constraining the size and shock speed to known values, was unusually low explosion energy. This inconsistency can be overcome by assuming the supernova goes off in a cavity created by the progenitor.

Figures 2-4 present the temperature, velocity, and density profiles from the model runs. Some of the complexity of the hydrodynamics of the transition from adiabatic to radiative can be readily seen. As the shock slows enough that radiative cooling causes the post-shock

gas to cool to $T \sim 10^4$ K, the shock loses pressure support and slows. The hot gas behind the shock then catches up with the shock, giving the shock renewed acceleration and resulting in extra compression and cooling in the cool shell. A reverse shock is initiated and propagates back into the hot gas then setting up the reverse shock/contact-discontinuity/forward shock structure familiar from situations in which a shock encounters a higher density medium such as a cloud. In this case it results simply from the dynamics of the transition to a radiative remnant. Note especially that after cooling sets in the hot gas in the remnant has a substantially higher velocity than the gas in the radiative forward shock.

Figure 5 shows the predictions of the numerical hydrodynamic models for the ratio O VI/C IV vs. shock speed. Also plotted are the results of steady radiative shock models kindly provided by John Raymond. The differences between the model results are clearly very large and point to the importance of dynamics in our calculations. A large contributor to the differences is the hot gas inside the remnant that constitutes the sole source of the O VI after the shock has slowed below the speed needed to produce O VI. Another factor is the contribution of the reverse shock to the C IV column, which becomes dominant for shock speeds below ~ 120 km s $^{-1}$.

Further complications for comparison of observational data to models is demonstrated by Figure 6 which shows the C IV 1548 Å and O VI 1032 Å absorption profiles calculated for a 4×10^4 yr after the SN explosion. O VI, coming primarily from hot gas in the remnant, has a single component centered at about 120 km s $^{-1}$. C IV, on the other hand, comes from both the forward shock and a thin layer on both sides of the reverse shock; thus it has two components. The extremely different nature of the absorption components for C IV and O VI cautions us against any simple component matching analysis of the observational data.

Conclusions

1. C IV and O VI absorption line observations can be powerful diagnostics of SNR characteristics: shock speed, ambient density, age - but interpretation of such results requires careful comparison with detailed models.

2. Steady radiative shock and fully time dependent SNR evolutionary calculations differ markedly in their predictions of C IV and O VI column densities vs. shock speed. This is primarily due to the presence of secondary shocks in the cold shell caused by the dynamics of shell formation and the presence of hot gas behind the cold shell in the SNR bubble.
3. Column densities for O VI and C IV compared to both steady shock models and hydro-dynamical SNR modeling, require the shock to be relatively slow ($\sim 100\text{-}170 \text{ km s}^{-1}$) to match the data.

Fig. 1.—*FUSE* data for the 1032Å line of O VI (red) and *IUE* data for the 1548Å line of C IV (green) for the three rapidly rotating stars in our *FUSE* dataset. Some or all of the absorption at $\sim 120 \text{ km s}^{-1}$ and $\sim 200 \text{ km s}^{-1}$ in the *FUSE* spectra is due to H₂. The *FUSE* data have been binned by a factor of three to increase signal-to-noise.

Fig. 2.—Evolution of the velocity profile in a supernova remnant in our calculation in which we attempt to simulate the Vela SNR. The legend indicates the time after the SN explosion for which each profile corresponds. Note how after $4.0 \times 10^4 \text{ yr}$ when the cold shell has formed, the fastest moving gas is interior to the shock at the location of the reverse shock. At these times this hot gas interior to the shell, which contains O VI, may have a velocity larger than the outer shock speed.

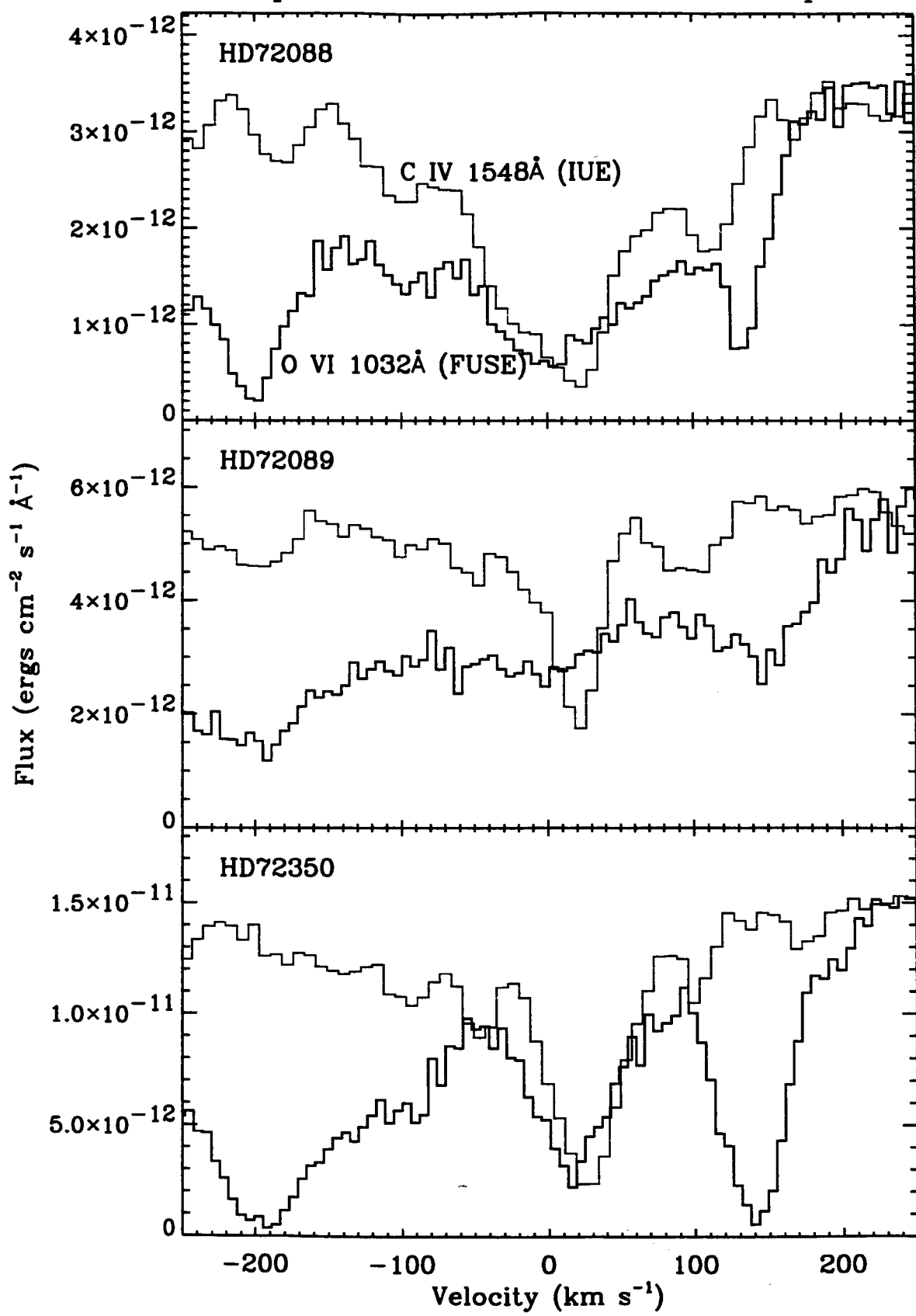
Fig. 3.—Same as Fig. 2, but the temperature. Note the formation of the cool shell, the thin radiative outer shock and the reverse shock that forms between $t = 3.5 \times 10^4 \text{ yr}$ and $4.0 \times 10^4 \text{ yr}$ after the explosion.

Fig. 4.—Same as Fig. 2, but the density. After formation the cool shell expands over time. The dense cold part of the shell is just behind the forward shock. The contact discontinuity can be seen best in the last profile where the density begins to drop behind the outer shock, flattens somewhat then drops again sharply at the inner (reverse) shock.

Fig. 5.—Ion column density ratio vs. shock speed. Here the large differences between the steady shock and hydrodynamical results are demonstrated. The colored dots correspond to the times on Figs. 2–4. The loop in the curve is due to the slowing of the shock after going radiative and subsequent re-acceleration after the hot gas in the expanding bubble catches up with the shock.

Figure 1

FUSE/IUE Data for Vela SNR Stars
Comparison of O VI and C IV Absorption



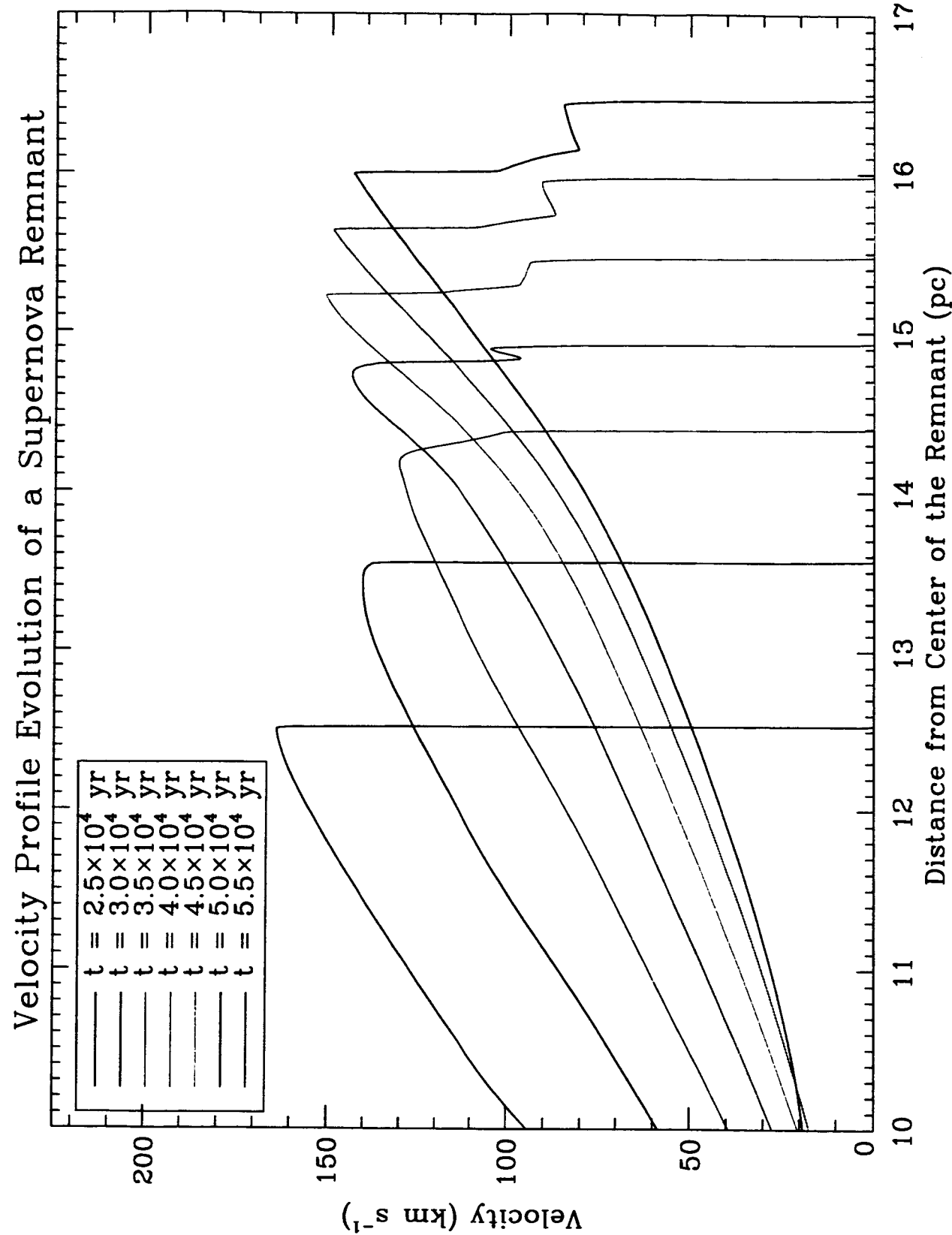


Figure 2

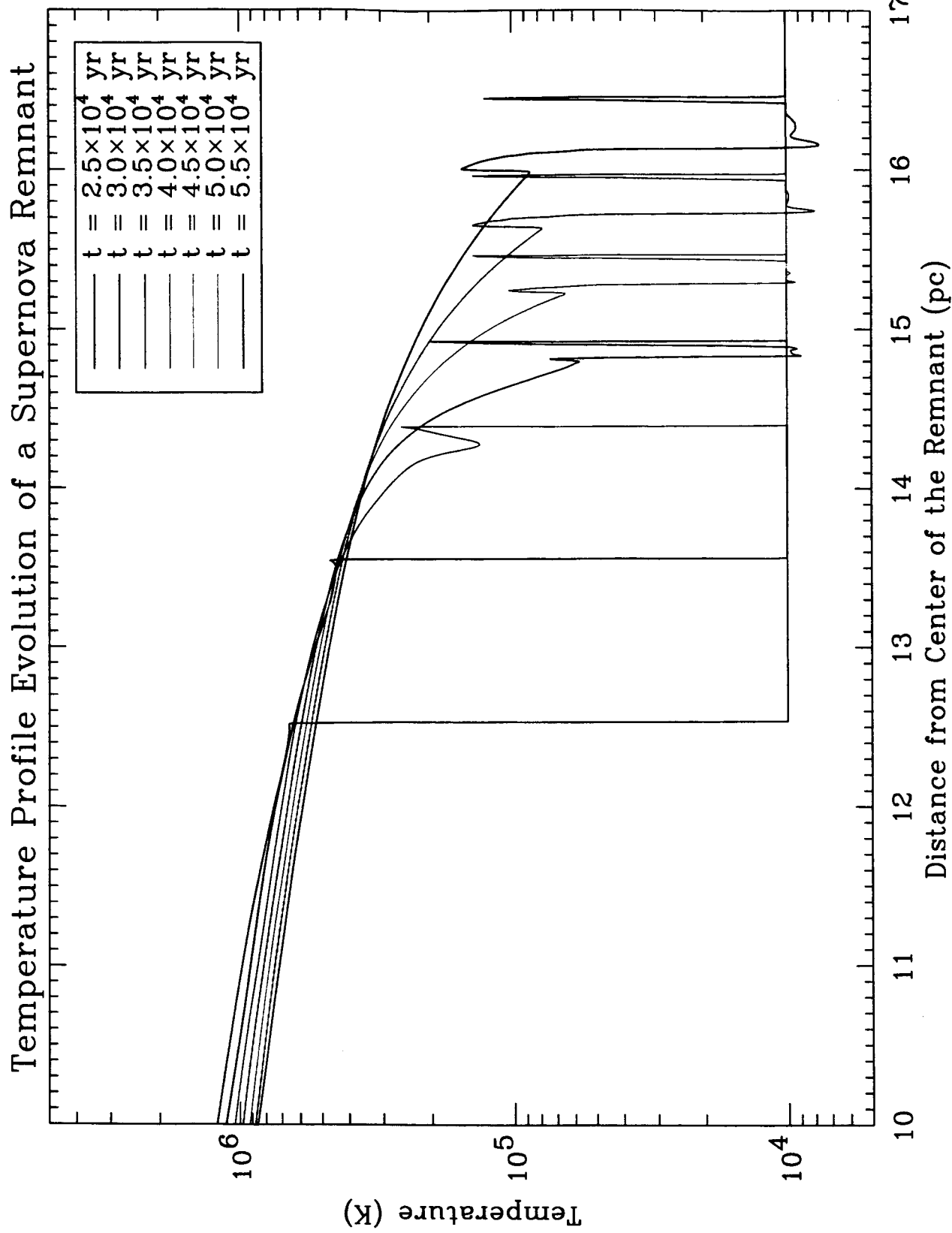
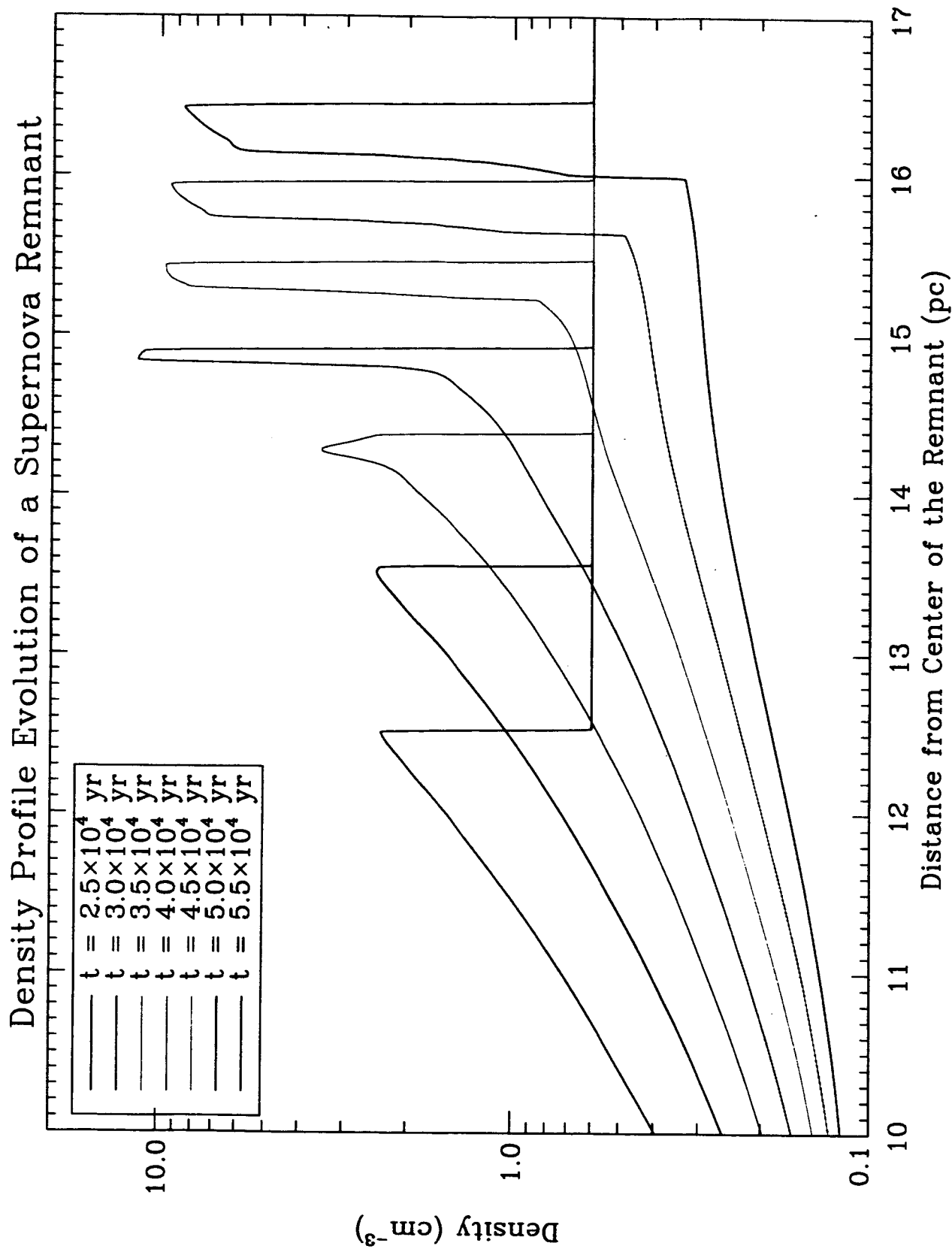
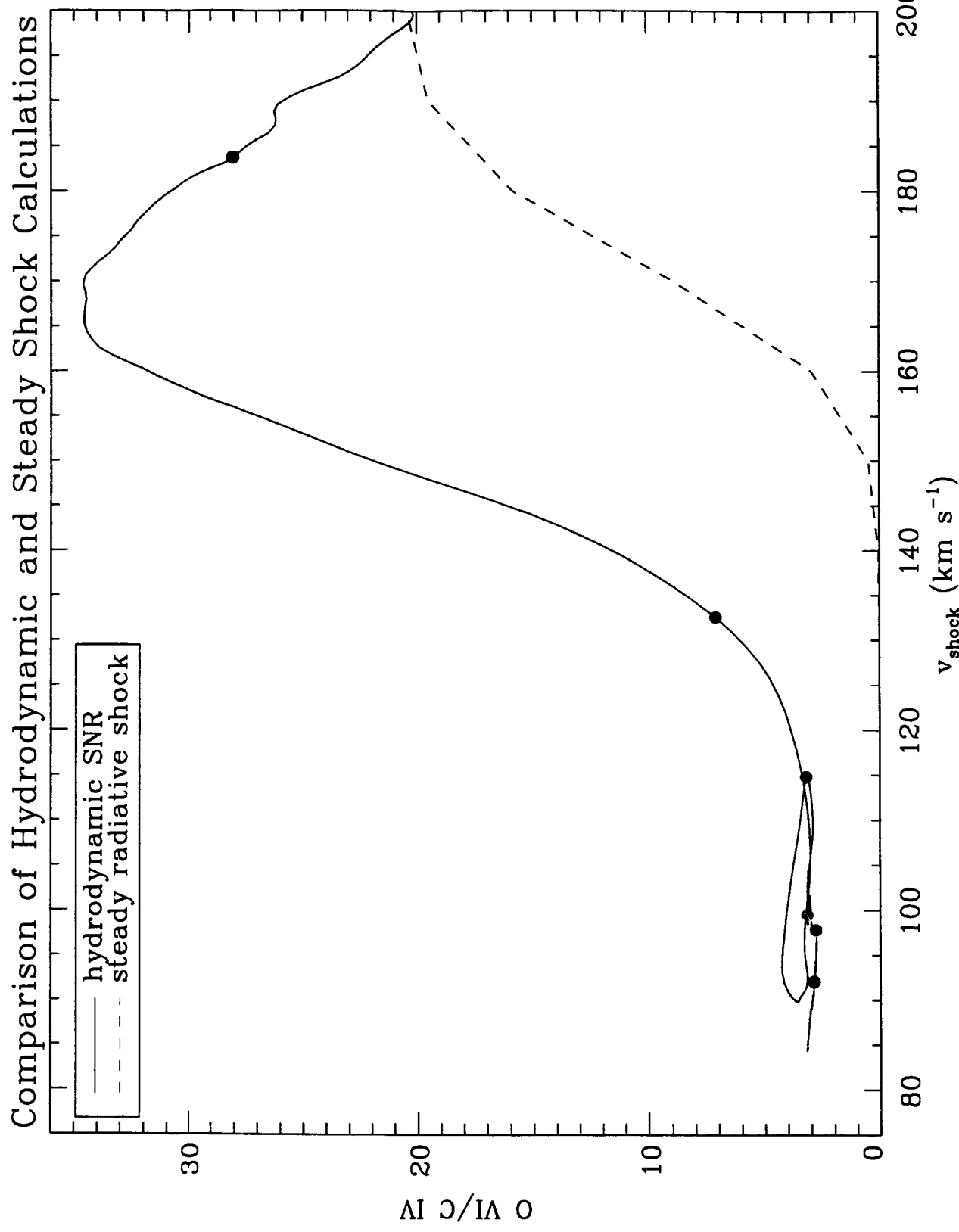


Figure 3

Figure 4





Example of Calculated C IV and O VI Absorption Profiles

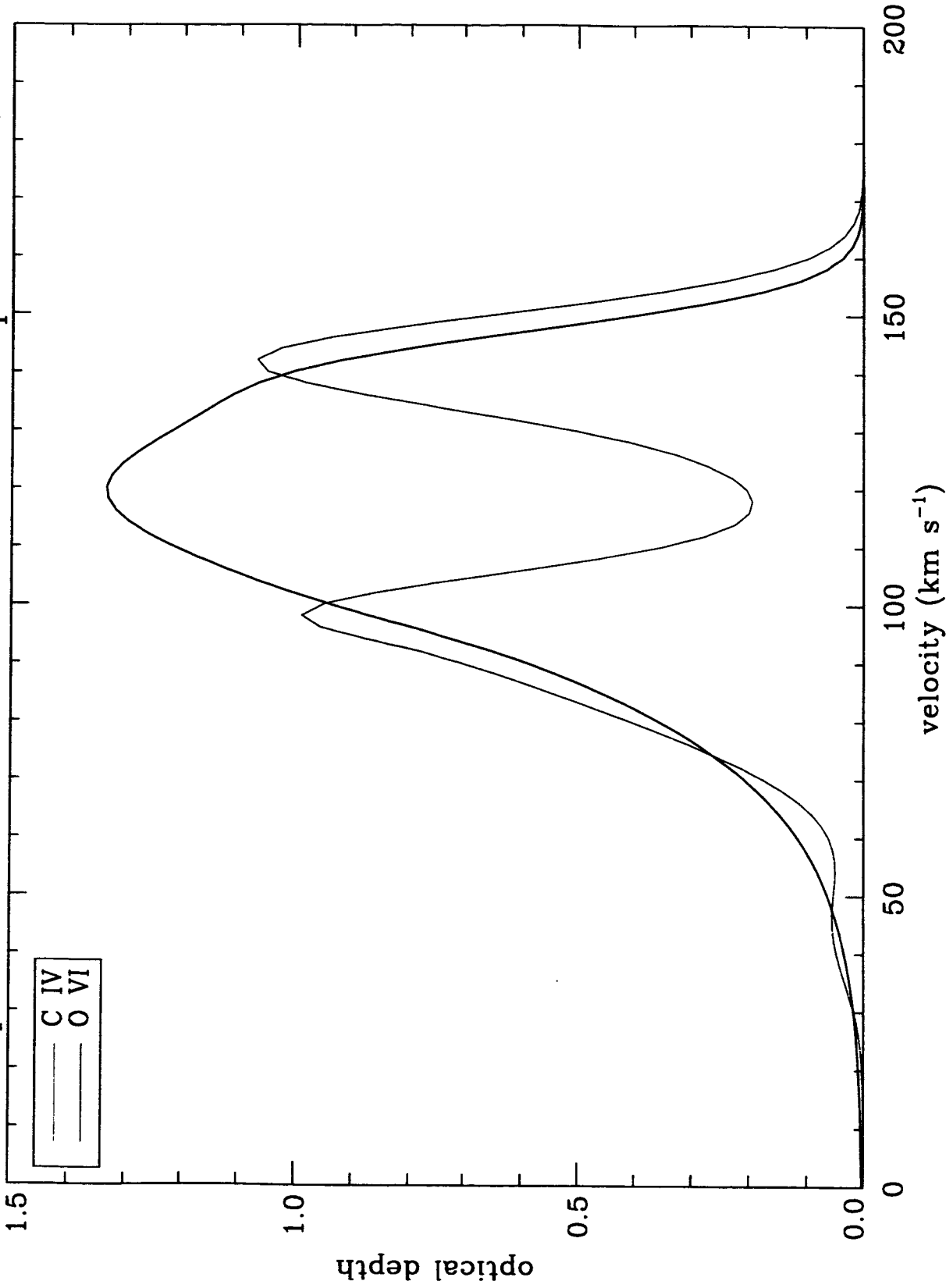


Figure 6